ARTICLE IN PRESS

International Journal of Hydrogen Energy xxx (xxxx) xxx

Contents lists available at ScienceDirect

International Journal of Hydrogen Energy

journal homepage: www.elsevier.com/locate/he

Control of wind energy conversion systems with permanent magnet synchronous generator for isolated green hydrogen production

Eduardo Rausell [a,*], Santiago Arnaltes [b], José Luis Rodríguez [b], Marcos Lafoz [a], Gustavo Navarro [a]

[a] CIEMAT, Spanish National Research Centre on Energy, Environment and Technology, 28040, Madrid, Spain
[b] Electrical Engineering Department, Carlos III University of Madrid, Av. de La Universidad 30, Leganés, 28911, Madrid, Spain

A R T I C L E I N F O

Handling Editor: Ibrahim Dincer

Keywords:
Green hydrogen
Alkaline electrolyzer
Permanent magnet synchronous generator
Wind turbine
Power converters control

A B S T R A C T

This paper addresses the design and analysis of the control system for a Wind Energy Conversion System (WECS) with a Permanent Magnet Synchronous Generator (PMSG) and its application for isolated green hydrogen production. The designed control maximizes the wind turbine (WT) power generation by regulating the electrolyzer current consumption, where the electrolyzer operates as a controlled load, ensuring power balance in the system and enabling the generation of maximum power from the WECS without the use of any energy storage system. The system involves directly integrating a WECS with an alkaline electrolyzer (AEL), and its configuration includes a WT with a PMSG, an AC/DC voltage source converter (VSC) acting as the generator side converter (GSC), and a DC/DC converter acting as the electrolyzer side converter (ESC) with Maximum Power Point Tracking (MPPT) control for the WT. The proposed control system has been fully modeled and tested through simulations in Matlab/Simulink, demonstrating its reliable performance under variable wind speeds. Simulation results illustrate how, over rated wind speeds, the pitch control limits the rotational speed and power to their maximum values, and at under rated wind speeds, the ESC control regulates the AEL current following the MPPT of the WT, while the GSC control maintains the DC bus voltage at its designated nominal value. Overall, the proposed control system shows robust and effective performance across the entire range of possible operational points, ensuring no wind generation power losses by following the maximum power point.

1. Introduction

The transition to achieve a net-zero emissions balance requires continuous research into sustainable and low-carbon energy alternatives. In this context, hydrogen has emerged as a solution to address the challenges of this transition. Hydrogen could be produced through different methods, among others, from fossil energy sources, also known as grey hydrogen. Almost 95% of hydrogen is produced from natural gas reforming which result in large CO2 emissions, approximately 11 tons of CO2 per ton of hydrogen [1]. Therefore, green hydrogen, produced through electrolysis powered by solar and wind energy, holds significant potential as a clean energy carrier, due to its low environmental impact and its versatility to decarbonize critical sectors such as transportation and chemistry industry [2,3].

However, the deployment of green hydrogen technologies faces several challenges. One of the most important is the production cost compared to other hydrogen production methods.

Currently, the production cost of grey hydrogen is around 0.8–1.6 €/kg and green hydrogen is above 3 €/kg [2]. Thus, the current objective of researchers and manufactures is to reduce production costs to be economically competitive. Governments are supporting and focusing their investments on the deployment of technologies related to green hydrogen. A clear example is the EU Hydrogen Strategy, which has an estimated budget of approximately 180–470 billion euros for the period of 2020–2050 [4]. To reduce the production cost of these technologies, it is necessary to decrease the cost of electrolyzers, lower electricity prices, and increase the operating hours of the electrolyzer (hybridization of renewable energies or storage) and its efficiency. For these reason, green hydrogen implies the continue searching of the optimal combination of renewable energies with electrolyzers. The optimal conversion of renewable energies into hydrogen can be achieved, among others, by means of [5].

* Corresponding author.
E-mail address: 100464931@alumnos.uc3m.es (E. Rausell).

https://doi.org/10.1016/j.ijhydene.2024.06.347
Received 30 November 2023; Received in revised form 21 June 2024; Accepted 25 June 2024
Available online 31 July 2024

1. Optimal sizing the capacity ratio between the electrolyzer and the electricity generation source [6].
2. Production of hydrogen not only in areas with grid connection but isolated from the grid [7].
3. Increase of the capacity factor (understood as the hydrogen produced annually over the rated capacity production) by means of the use of energy storage to optimize the production [8].
4. Use of advanced power electronics topologies and control strategies in order to improve the performance and efficiency and reduce equipment [9].

The paper is mainly focused on the second and fourth measures, analyzing an isolated system to produce hydrogen through electrolyzers using renewable energies and designing a novel control for the specific system configuration to reduce equipment. The control strategy for green hydrogen production in off-grid systems has been studied in the literature by several authors, who have developed system configurations using various renewable energy sources and energy storage solutions.

The authors in Refs. [10–12] present a configuration for isolated green hydrogen production using photovoltaic (PV) solar energy. The PV array power is connected to the electrolyzer through a DC/DC buck converter. Buck converter is required to step down the voltage since the electrolyzer operates at lower voltages and higher currents than the PV array. The system also incorporates a maximum power point tracking (MPPT) algorithm with the aim of maximizing solar generation and, consequently, hydrogen production. The studies have confirmed the effective operation of this configuration and the simplicity of its control.

In [13–15], another configuration is proposed for solar energy generation, where the PV array is directly connected to a PEM electrolyzer without the use of power electronics. The purpose of this configuration is to eliminate the MPPT algorithms and DC/DC converters in order to reduce power electronics (PE) costs and losses. However, this configuration presents limitations in terms of operation range and challenges in terms of system sizing and design, not being able to achieve a high capacity factor. To maximize the generated solar energy, the electrolyzer must be designed in such a way that its V–I curve aligns with the maximum power points of the PV array. Since matching the V–I curve of the electrolyzer to all the maximum power points is complex, efforts are made to match the points for the irradiances that generate the highest annual energy. The study concludes that the system performs satisfactorily, even through fast and continue generation varia tions. Furthermore, despite the absence of MPPT, the system efficiency is close to the theoretical value, and there's substantial cost savings due to power electronics elimination. Nevertheless, it should be noted that abrupt generation changes directly impact the degradation of the electrolyzer.

The system proposed in Refs. [16–19] presents hydrogen generation through isolated wind energy conversion systems (WECSs).

The configuration is based on a wind turbine (WT) with a permanent magnet synchronous generator (PMSG) where the generator side converter (GSC) is a diode rectifier connected to a DC link by a DC/DC converter, operating with MPPT control. The DC link is also connected to a fuel cell, batteries, and an electrolyzer, all with their respective DC/DC converters. There's also a controlled DC/AC converter operating as a load side converter (LSC) to power an AC load. The system operates with the strategy that the battery and fuel cell maintain the voltage of the DC link when there are imbalances between the WT generation and the electrolyzer and load demand. This configuration, which represents a microgrid by itself, demonstrates favorable results and the fast response of hydrogen technologies to changes in power during operation. However, this system requires a significant number of devices, and its control and operation are quite complex.

The connection of electrolyzers to WECS is more challenging than connecting them to PV solar systems. This is due to the need for additional power electronics and control, as well as the higher level of power oscillation generated by the wind energy resource. However, the current electrolyzer technologies can operate under these power oscillations.

Alkaline and PEM electrolyzer technologies are well-suited to support the intermittent and fluctuating nature of wind energy generation due to their specific technical characteristics. PEM electrolyzers have rapid response times, able to adjust their current consumption at a rate of 100% per second [20], allowing them to go from standby mode to full capacity in just 1 s, making them highly responsive to the variable output of wind power. They also exhibit high efficiencies, often around 61–70% [21]. AEL, while having slightly longer response times and adjusting at a rate of 0.2–20% per second [20], are still capable of adapting to changes in wind energy supply, with efficiencies ranging from 63 to 73% [21]. Both types of electrolyzers maintain high efficiency even when operating at partial loads, which is crucial for handling the variability of wind energy. PEM electrolyzers also have the widest operating range, from 0% to 160% of their nominal capacity, compared to 10%–110% for AEL [20]. Although PEM electrolyzers offer better dynamic response and flexibility, the capital cost of AEL technology is currently considerably lower. AEL costs range from 437 to 700 €/kW, while PEM costs range from 613 to 1160 €/kW [21].

PEM and AEL have modular designs based on stacks of cells, allowing scalable hydrogen production that can be adjusted to optimize the capacity ratio between the electrolyzer and the electricity generation source. Their characteristics enable them to endure frequent start-stop cycles and load changes, which are common with renewable energy sources. These features make PEM and AEL suitable for integration with WECS, providing a reliable method to convert and store renewable energy as hydrogen [22], or to provide grid system services such as frequency or voltage control [23].

The objective of this paper is to develop and present a comprehensive model, as well as to validate through simulation and analysis a novel control for an isolated green hydrogen production system from a WECS. The proposed approach involves the direct integration of a WT with an electrolyzer. As shown in Fig. 1, the system configuration consists of a WT with a PMSG, an AC/DC voltage source converter (VSC) acting as the generator side converter (GSC) to maintain the DC link voltage, and a DC/DC converter acting as the electrolyzer side converter (ESC) regulating the AEL current consumption. Although this system configuration has been considered for dimensioning, economic viability, and optimization studies [24] (showing significant reductions in the LCOH depending on the sizing of the wind turbine and the electrolyzer, as well as the availability of wind energy resources in the area) the control aspect of the system has not yet been addressed in the literature. Therefore, the designed control system maximizes WT power generation by regulating the electrolyzer current consumption, where the electrolyzer operates as a controlled load, ensuring power balance in the system and enabling the generation of maximum power from the WECS without the use of any energy storage systems. The ESC operates with a current reference according to the MPPT control of the wind turbine. The analysis of the system, based on simulations, has been accomplished using a mathematical model for an a AEL found in the literature [25].

It is important to note that, unlike other literature studies on isolated WT green hydrogen systems [26,27], this configuration, as shown in Fig. 1, does not utilize energy storage to support the regulation the DC link that couples the WT and the AEL. On the one hand, not using energy storage helps to reduce the number of devices and the overall system cost and therefore the cost of energy, which impact directly in the cost of hydrogen production. On the other hand, without the use of energy

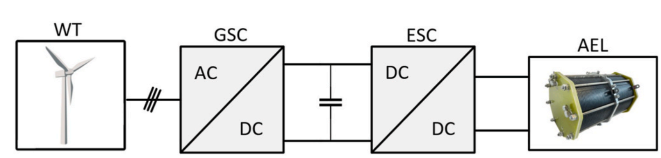

Fig. 1. Proposed Isolated WECS Green Hydrogen production system. (For interpretation of the references to colour in this figure legend, the reader is referred to the Web version of this article.)

storage, the electrolyzer may experience abrupt changes in generation, directly impacting its degradation and service life [28]. Nevertheless, this paper doesn't address this particular problem, which will be studied in future works.

The paper is organized as follows. In Section 2 models of the WT, PMSG and AEL are presented. Section 3 provides a comprehensive description of the proposed control strategies of the complete system. In Section 4 the validation of the proposed system is performed through simulations using Matlab/Simulink, and the results are shown. Finally, the conclusions derived from the study are discussed.

2. System model

In this section the model of the complete system is described.

In Fig. 2 a complete system scheme is presented. As mentioned before the system could be divided in 5 different elements or subsystems. The WT model provides the mechanical torque to the PMSG that transforms the mechanical power into AC power. Then the GSC rectifies the AC power into DC maintaining the DC link voltage constant. Finally, the DC link is connected to the ESC that controls the current consumption of the electrolyzer, maximizing the WT power generation.

2.1. Wind turbine model

The wind turbine is modeled following its power conversion model [29]. The mechanical power of the WT is expressed as

$$P_m = \frac{1}{2}\rho A v_{\text{wind}}^3 c_p(\lambda, \beta) \tag{1}$$

where A is the turbine swept area, v_{wind} is the wind speed, ρ is the air density and c_p is the performance coefficient of the turbine, which is a function of two parameters, the blade pitch angle (β) and the tip speed ratio of the rotor blade speed to wind speed (λ). For modelling $c_p(\lambda,\beta)$ the following analytic equation is used [30]:

$$c_p(\lambda,\beta) = c_1\left(\frac{c_2}{\lambda_i} - c_3\beta - c_4\right)e^{-\frac{c_5}{\lambda_i}} + c_5\lambda \tag{2}$$

$$\frac{1}{\lambda_i} = \frac{1}{\lambda + 0.08\beta} - \frac{0.035}{\beta^3 + 1} \tag{3}$$

Fig. 3 shows the $c_p - \lambda$ characteristics for different β values. As can be observed, the maximum performance coefficient (c_{pmax}) is 0.48 when $\beta_{\text{opt}} = 0$ and $\lambda_{\text{opt}} = 8.1$. Fig. 3 shows that by varying β and λ values the mechanical power of the wind turbine can be regulated. Therefore, the maximum power point can be tracked by adjusting the rotational speed of the wind turbine following the incident wind speed in order to operate at point c_{pmax}.

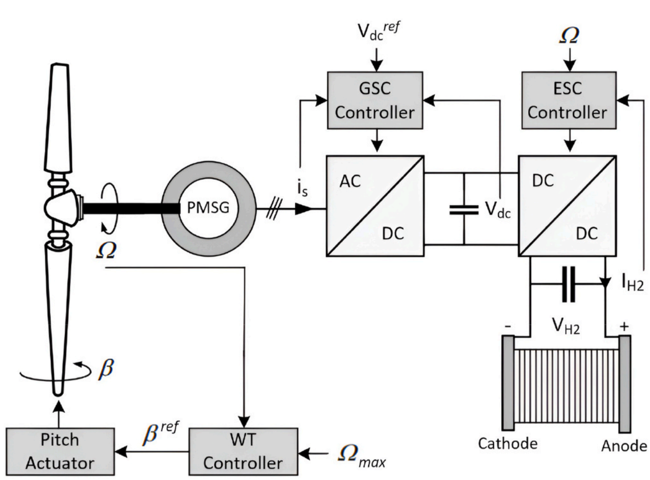

Fig. 2. Complete scheme of the proposed system.

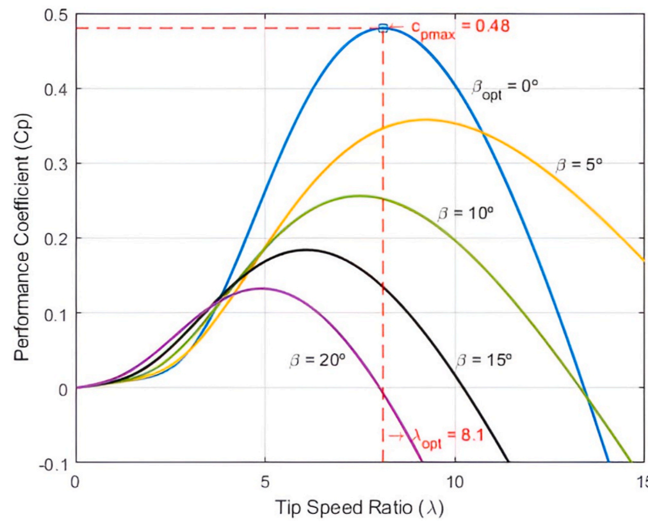

Fig. 3. Performance coefficient $c_p(\lambda,\beta)$ characteristics.

In Fig. 4, the wind turbine power characteristics, and the maximum power locus (curve ABCD) are represented. At point A, it is observed that for wind speeds below 6 m/s, the rotational speed remains constant and equal to the minimum Ω_{min}. The segment BC corresponds to the maximum power point tracking, with a cubic function of the rotational speed as described by equation (5) until reaching point C.

$$\lambda_{opt} = \frac{\Omega_{opt} R}{v_{\text{wind}}} \rightarrow v_{\text{wind}} = \frac{\Omega_{opt} R}{\lambda_{opt}} \tag{4}$$

$$P_{m,MPPT} = \frac{1}{2}\rho A\left(\frac{\Omega_{opt} R}{\lambda_{opt}}\right)^3 c_{\text{pmax}} = K_{MPPT}\Omega_{opt}^3 \tag{5}$$

At point C, the rotational speed is at its maximum Ω_{max}, and in segment CD, the rotational speed remains limited to this maximum value, while the wind speed increases until it reaches its nominal value at D. For wind speeds exceeding the nominal value, the pitch control is activated to maintain constant mechanical power, while limiting the rotational speed to its maximum value. The power characteristics and maximum power locus of the wind turbine are employed within the control system presented in Section 3.

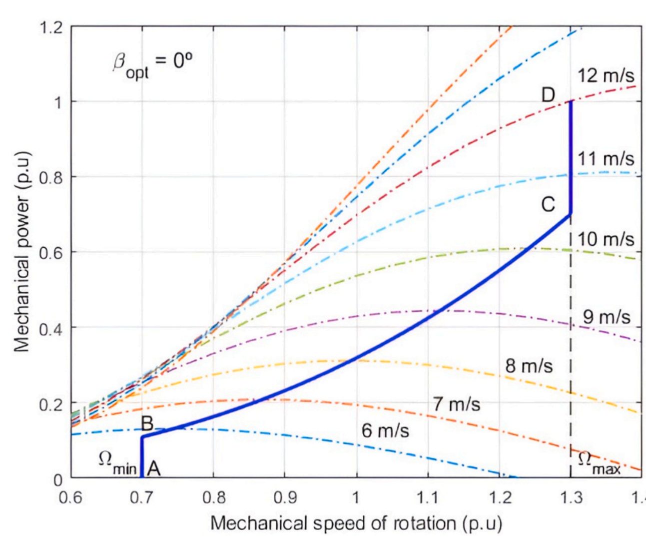

Fig. 4. Wind turbine power characteristics and maximum power locus.

2.2. PMSG model

The PMSG is modeled in the dq rotating frame, oriented to the rotor, in order to implement a dynamic control system [31]. In this case, it is a surface-mounted PMSG where the control strategy involves a current control in phase with the electromotive force ($i_{sd} = 0$). Thus, the electrical equations of the surface-mounted PMSG can be expressed as [28].

$$u_{sd} = -R_s i_{sd} - L_s \frac{d}{dt} i_{sd} + \omega_r L_s i_{sq} \tag{6}$$

$$u_{sq} = -R_s i_{sq} - L_s \frac{d}{dt} i_{sq} - \omega_r L_s i_{sd} + \omega_r \psi \tag{7}$$

where u_{sd} and u_{sq} are the stator voltages in dq coordinates, i_{sd} and i_{sq} are the stator currents, R_s and L_s are the generator resistance and inductance, ψ is the magnetic flux linkage established by the magnets and ω_r is the electrical rotating speed related to the mechanical rotor speed through the number of pole pairs (p) as $\omega_r = p\Omega$. The electromagnetic torque of the PMSG, considering that it is a surface mounted permanent magnet generator, can be express by the following equation [32]:

$$T_{em} = \frac{P_{em}}{\Omega} = P_{em}\frac{p}{\omega_r} = \frac{3}{2} p \psi i_{sq} \tag{8}$$

Equations (6) and (7) show that the dq currents components can be controlled by the applied stator voltages, and equation (8) shows that the electromagnetic torque can be controlled by the stator current q component. Therefore, in this system, in order to mantain the DC link voltage, as stated before, the reference current i_{sq} will be set by a voltage DC voltage controller, as it will be shown below.

2.3. AEL model

The AEL is modeled using the Ulleberg empirical equation [25], which has been derived from the voltage-current (V–I) curves of an actual alkaline electrolyzer cell. The electrochem-ical response of the cell is given by

$$U_{\text{cell}} = U_{\text{rev}} + \frac{r_1 + r_2 T}{A} I + s\log\left(\frac{t1 + t2/T + t3/T^2}{A} I + 1\right) \tag{9}$$

where U_{rev} is the reversible cell voltage (minimum applied voltage to split H_2O into H_2 and O_2), A is the cell area, T is the working temperature, r_n are ohmic resistance parameters, s and t_n are overvoltage and temperature overvoltage coefficients and I is the current absorbed by the cell. Equation (9) is valid for a single cell electrolyzer. To model a full electrolyzer with multiple cells, we need to multiply the number of cells in series (n_c) by equation (9).

Fig. 5 shows the V–I curves of the electrolyzer cell at dif-ferent temperatures. As observed, cell voltage is lower at higher temperatures; therefore, voltage efficiency is improved Voltage efficiency is expressed as [33].

$$n_V = \frac{U_{th}}{U_{\text{cell}}} \tag{10}$$

Where U_{th} represents the thermoneutral voltage that includes the heat energy associated with the change in entropy and equals 1.48 V under standard conditions.

However, higher temperatures have a negative impact on the aging and service life of the electrolyzer. Additionally, it can be observed that cell voltage increases with current density. Nevertheless, operating at lower current density also reduces the hydrogen production rate (as shown in equation (11)), increasing the specific cost of an electrolyzer. It is important to note that the operation and design of an electrolyzer are focused on achieving an optimal balance between efficiency, service life, and cost [34].

The hydrogen production rate of the electrolyzer can be expressed as

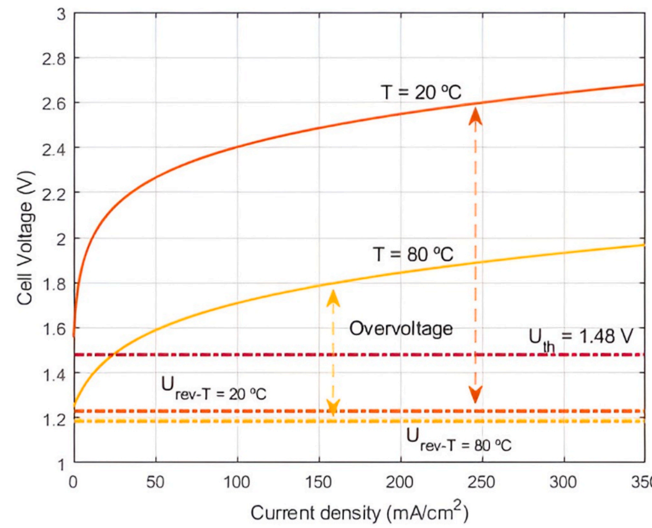

Fig. 5. V–I curves for an electrolyzer cell at different temperatures.

[35].

$$\dot{n}_{H_2} = n_F \frac{n_c I}{zF} \tag{11}$$

where z is the number of electrons transferred per reaction, F is the Faraday constant, n_c is the number of cells in series and η_F is the Faraday efficiency [34] given by the following empirical expression

$$\eta_F = \frac{(I/A)^2}{f1 + (I/A)2} f_2 \tag{12}$$

where f parameters are empirical parameters related to Faraday efficiency. Faraday efficiency represents the ratio of the real hydrogen produced and its theoretical maximum. This efficiency accounts electrical current losses and other H_2 losses.

Fig. 6 shows the Faraday efficiency at different temperatures. The efficiency increases with current and improves at lower temperatures.

3. Proposed control system

In this section the proposed control system is fully described. The control ensures the proper operation of the system under continue variations of wind speed. There are three control subsystems: WT Control,

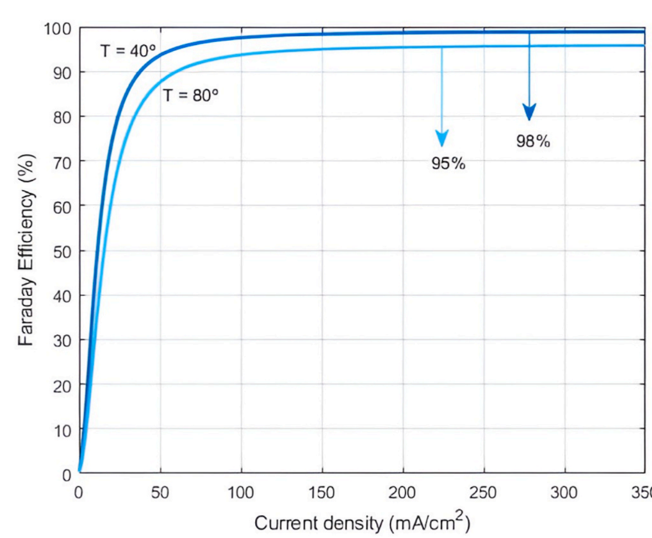

Fig. 6. Faraday efficiency for different temperatures.

GSC Control and ESC Control.

3.1. WT control

The WT control, based on the pitch control, limits both the rotational speed and mechanical power of the wind turbine to their respective maximum values. This control is automatically activated when the rotational speed of the wind turbine exceeds its rated value. The control is achieved through the adjustment of the blade pitch angle. As discussed in section 2.1, by varying the angle β, the mechanical power of the wind turbine is controlled.

The mechanical equation of the WT is expressed as [36].

$$\frac{d\Omega}{dt} = \frac{1}{J}(T_{WT} - T_{em}) \tag{13}$$

where J is the inertia, Ω is the rotational speed and T_{WT} and T_{em} are the WT torque and generator torque respectively. Equation (13) shows that if the WT power is higher than the electrolyzer power, the rotational speed will increase and if the electrolyzer power is higher than the WT power, the rotational speed will decrease. Thus, when the WT power and the electrolyzer power are equal the rotational speed is constant, and the power is balanced. This balance is achieved by means of the pitch control when wind velocity is over rated.

Fig. 7 illustrates the scheme of the implemented pitch control. When the measured rotational speed (Ω) is higher than the maximum value (Ω_{max}), a reference value of the blade pitch angle (β_{ref}) is generated and sent to the pitch actuator. The dynamics of the pitch actuator are modeled as a first-order system with ($\beta_{re\ f}$) as input and (β) as output [37]. The model calculates the rotational speed of the pitch angle, which is bounded between its maximum and minimum values. Then, this value is integrated to obtain the pitch angle, which is also constrained between the values β_{min} and β_{max}. It is important to note that, in this model, the pitch actuator is limited at $\pm$ 10°/s to avoid excessive mechanical load in the blade.

3.2. GSC control

The GSC objective is to maintain the DC-link voltage at a reference value under power fluctuations in the system. It has to be noted that the control strategy, based on maintaining constant DC voltage, means that the generator supplies exactly the power demanded by the electrolyzer. To achieve this, it regulates the active power produced by the PMSG through the control of the q-component of the stator current (i_{sq}). This component is directly linked to the active power, as described in equation (8). The reference value of i_{sq} (i_{sq}^{ref}) is determined by a DC voltage controller. If the power generation increases, the DC-link voltage will increase, and the DC voltage controller must then increase i_{sq}^{ref}, providing more power to the electrolyzer.

Therefore, in order to transfer all the power generated in the WT, the DC-link voltage should be maintained at a constant value by using a current control. Thus, the DC-link controller can be defined based on [38].

$$C\frac{dV_{DC}}{dt} = \frac{P_{WT}}{V_{DC}} - \frac{P_{H2}}{V_{DC}} \tag{14}$$

where C is the capacitance of the DC-link capacitor, V_{DC} is the DC-link voltage P_{WT} and P_{H2} are the power of the wind turbine and electrolyzer, respectively. If P_{WT} and P_{H2} are equal, there will be no change in the DC-link voltage. The measured error in the DC-link voltage is used to determine the reference value of i_{sq}^{ref} via the PI controller shown in Fig. 8. Regarding the stator current d-component, there are various criteria for its selection. In this paper, the “maximum torque per ampere” criterion has been implemented, where $i_{sd}^{ref} = 0$ [29].

Once i_{sq}^{ref} and i_{sd}^{ref} are determined, the current control loop regulate the stator currents by comparing the reference values with the measured values. Then, the stator voltages references u_{sq}^{ref} and u_{sd}^{ref} are generated using PI controllers.

Finally, to generate a switching signal for the IGBTs of the GSC a pulse width modulation (PWM) is utilized. The GSC control scheme is shown in Fig. 8.

3.3. ESC control

The ESC control acts as the MPPT controller for the wind turbine, ensuring that it operates within the maximum power locus as shown in Fig. 4. To achieve this, the current consumption of the electrolyzer is controlled, accelerating or decelerating the wind turbine until it reaches the rotational speed corresponding to the maximum power point.

Fig. 9 shows the ESC control scheme. The reference rotational speed is obtained from the mechanical power of the wind turbine and the maximum power locus. This first loop generates the reference current of the electrolyzer (I_{H2}^{ref}) by comparing the reference rotational speed (Ω_{ref}) with the measured rotational speed (Ω) and using a PI controller.

Then the second loop controls the current absorbed by the electrolyzer. The measured electrolyzer current (I_{H2}) is compared with the reference current of the electrolyzer (I_{H2}^{ref}) and the ESC duty cycle is generated using a PI controller.

It is important to note that the WT control and the ESC control are coordinated. In the case that the WT provides a certain power to the DC-link, higher than the maximum power to be managed by the AEL, the rotational speed of the WT keeps increasing. At some point, the pitch control will act to control the rotational speed taking the power generation down. Thus, over rated wind velocity, when the measured rotational speed tend to exceed the maximum rotational speed, the ESC control saturates and it does not contribute to the overall control. Consequently the maximum electrical load is applied to the generator

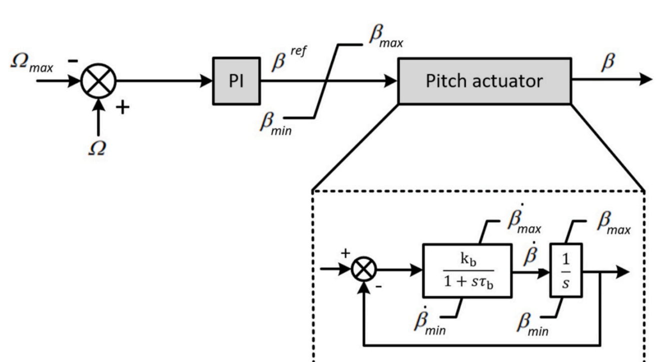

Fig. 7. WT pitch control scheme.

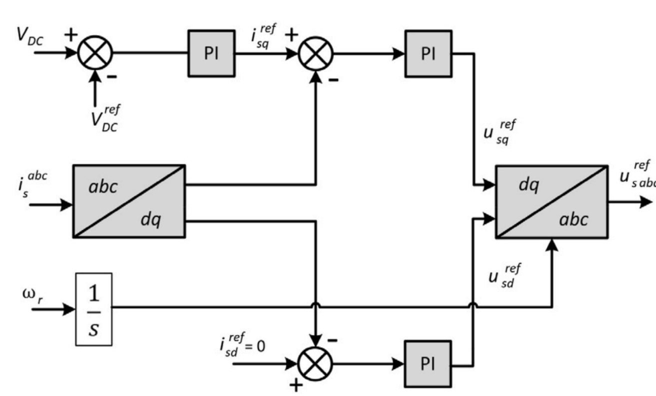

Fig. 8. GSC control scheme.

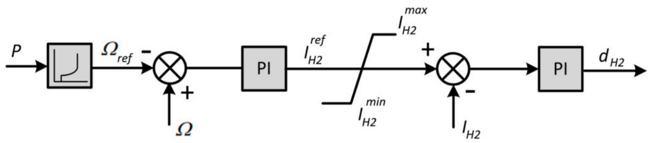

Fig. 9. ESC control scheme.

and the rotational speed must be controlled through the pitch control. Subsequently, when the rotational speed is lower than the maximum rotational speed, the WT control saturates, and the blade pitch angle is kept at 0° degrees. Then, the optimal rotational speed, producing to the WT maximum power, is controlled through the loading of the generator via the electrolyzer current.

4. Simulation results

In this section, the simulation results of the proposed system are presented and discussed. A comprehensive simulation model in Matlab/Simulink has been implemented for the system validation using the parameters of a 1.5 MW WT [39] and 1.5 MW AEL [25]. The simulation parameters are given in Appendix A.

4.1. Step from full power to partial load

In this simulation case, the response to a step change in wind speed, from rated wind velocity (12 m/s) to a value under rated, is being tested. The WT is working initially at nominal rotational speed (30.18 rpm) and nominal power (1.5 MW). The wind speed changes from 12 m/s to 11 m/s at t = 2 s, as shown in Fig. 10.

The objective of this simulation is to validate the GSC and ESC control responses, analyze the responses of the WT and AEL to a sudden change in wind speed, and consequently, assess the effects of power generation and consumption from full power to a partial load. The ESC control must regulate the rotational speed of the WT until it reaches the corresponding speed at the maximum power point, through the control of the current demanded by the electrolyzer. The GSC control must maintain the voltage of the DC link at the reference value. As explained before, in this simulation, the pitch control becomes saturated because the rotational speed is equal to or lower than the nominal value. Consequently, the blade pitch angle will remain at 0° degrees.

As shown in Fig. 11, when the wind speed decreases, the rotational speed of the wind turbine begins to slow down. The electrolyzer current is kept at its maximum value to continue decelerating the rotational speed until it reaches the MPPT value.

Once this point is reached, the electrolyzer current is reduced to the level required to maintain the rotational speed at its MPPT value.

In Fig. 12, the DC link voltage and the i_{sdq} currents are presented. A small disturbance is observed in the DC link voltage. Initially the power generation reduction due to the wind velocity reduction tend to produce a power imbalance in the DC link, the generator current is increased to compensate the rotor deceleration due to the reduction of the wind velocity, as initially the current drawn by ESC does not change

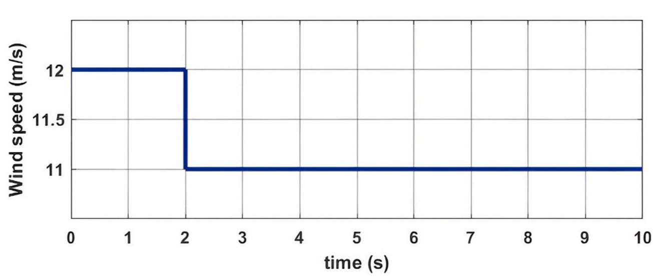

Fig. 10. Step from full power to partial load: Wind speed.

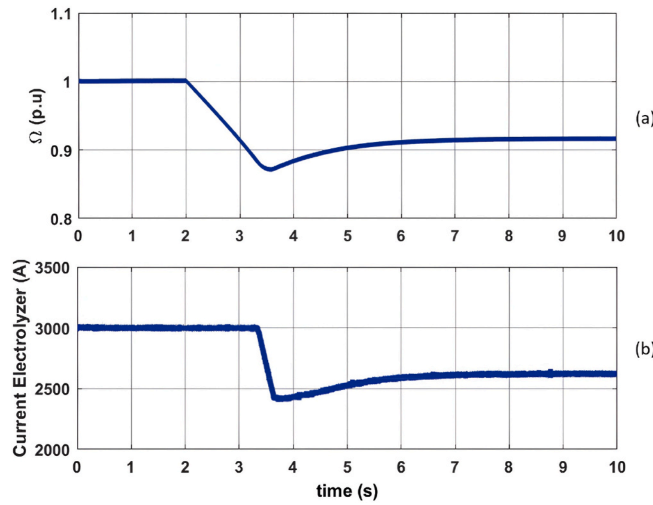

Fig. 11. Step from full power to partial load: (a) Rotational Speed (Ω in p.u). (b) Electrolyzer Current.

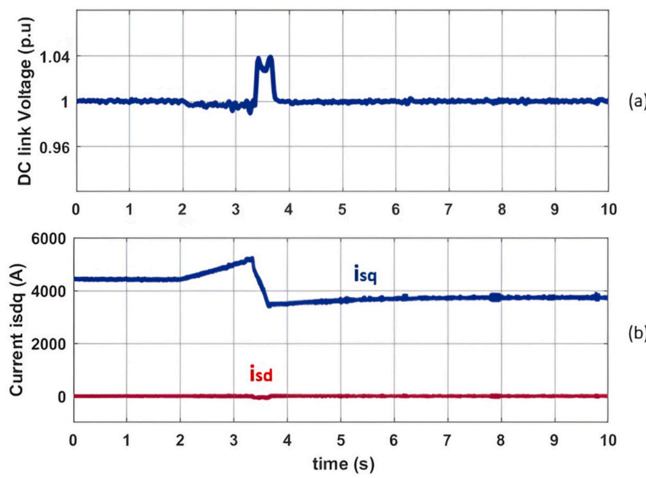

Fig. 12. Step from full power to partial load: (a) DC link Voltage. (b) PMSG stator currents in dq.

Nevertheless, as observed, the DC link voltage is maintained at its reference value under the severe power change by regulating the active power extracted from the PMSG, through the control of the q-component of the generator stator current. Also, note that despite the changes in the stator current q-component, the GSC stator current d-component is maintained at is reference value of zero. These tests show the proper operation of ESC and GSC controls.

4.2. Wind speed step at partial load

In this simulation case, the response to a step change in wind speed under rated is being tested. The wind speed changes from a value below its rated speed to another value still below its rated wind speed. The WT is working initially at the maximum power point of 27.7 rpm and 1.16 MW at 11 m/s. Then, as shown in Fig. 13, the wind speed changes from 11 m/s to 10 m/s at t = 2 s.

As shown in Fig. 14, similarly to the previous simulation, when the wind speed decreases, the rotational speed of the wind turbine starts to decrease as well. In this case, the electrolyzer current increases its value to decelerate the rotational speed rapidly until it reaches the Ω_{ref} value related to the MPPT. Once this point is reached, the electrolyzer current is reduced to the value required to maintain the rotational speed at its

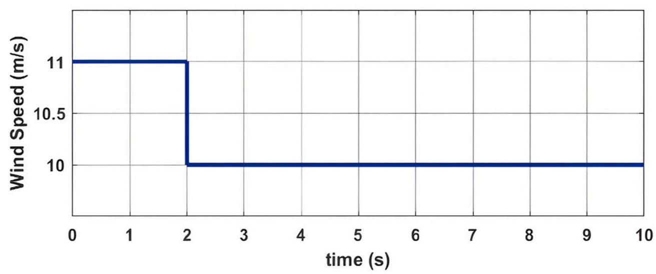

Fig. 13. Wind speed step from 11 m/s to 10 m/s.

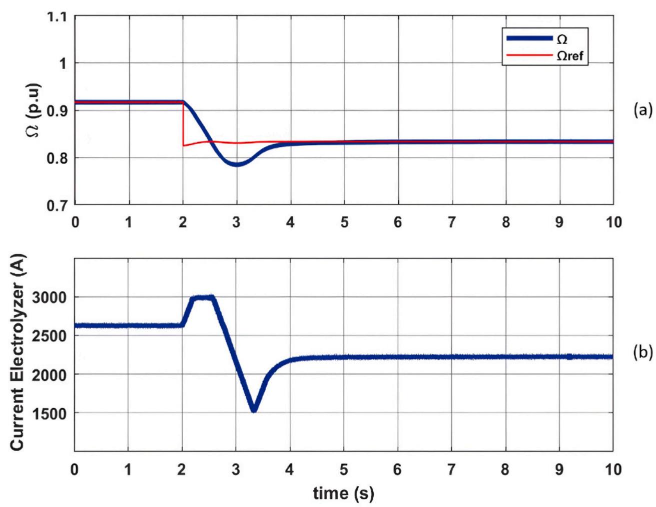

Fig. 14. Wind speed step at partial load: (a) Rotational Speed (Ω). (b) Electrolyzer Current.

MPPT value. As observed, it takes almost 2 s from the wind step to reach the Ω_{ref}.

In Fig. 15, the DC link voltage and the i_{sdq} currents are shown. Unlike the previous simulation, in this case, the disturbance in the DC link voltage is more significant due to the electrolyzer current change. As previously discussed, in this simulation, the electrolyzer current initially rises to decelerate the WT, followed by a subsequent decrease to maintain Ω_{ref}. Both of these changes create a disturbance in the DC link voltage. Nevertheless, it is important to highlight that the disturbance persists for only 1.5 s, its value is approximately ±0.05 p.u and is effectively regulated by controlling the stator current q-component. Also, note that despite the changes in the stator current q-component, the stator current d-component is maintained at is reference value of zero.

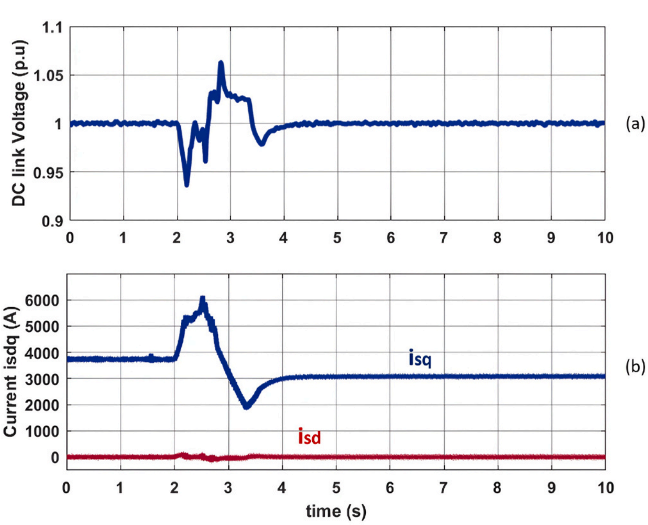

Fig. 15. Wind speed step at partial load: (a) DC link Voltage. (b) PMSG stator currents in dq.

4.3. Step from rated wind speed to wind speed above rated

In this simulation case, the response to a step change in wind speed, transitioning from its nominal value to a value above rated, is being tested. The WT is working initially at nominal rotational speed (30.18 rpm) and nominal power (1.5 MW). The wind speed changes from 12 m/s to 13 m/s at t = 2 s, as shown in Fig. 16.

The objective of this simulation is to validate the WT control system and analyze how both the wind turbine and pitch control respond to a sudden increase in wind speed exceeding its nominal value. In contrast to the other two simulations, in this case, the ESC control becomes saturated because the rotational speed exceeds its maximum value and the electrolyzer current cannot be increased over it nominal value. The wind turbine control must adjust the blade pitch angle to maintain the wind turbine's rotational speed at its maximum value and prevent it from exceeding the maximum power.

As shown in Fig. 17, when the wind speed increases, the wind turbine begins to accelerate. The electrolyzer current is maintained at its maximum value, and the pitch control starts increasing the blade pitch angle to limit the rotational speed at its maximum value. Once the pitch control manages to regulate the rotational speed to its maximum value, the blade pitch angle remains stable, ensuring that the power generated equals the maximum generation power.

In Fig. 18, the DC link voltage and the i_{sdq} currents are presented. As observed, there's an almost imperceptible disturbance in the DC link voltage at t = 2 s due to the wind speed step and the pitch control that control the power generation. Nevertheless, it is rapidly controlled through the current control, ensuring that the power generated and the power consumed are equal.

4.4. Step over rated wind speed

In this simulation the response to a step change in wind speed is being tested. The wind speed transitions from a value above its rated speed to another value still above its rated wind speed. Then, as shown in Fig. 19, the wind speed changes from 13 m/s to 14 m/s at t = 2 s.

As shown in Fig. 20, at t = 2 s, the rotational speed rises due to the wind disturbance, resulting in a sudden increase in power generation. The blade pitch angle increases from its previous value to restrict the rotational speed and generation power to their maximum values.

In this scenario, it takes 12 s to reach the nominal rotational speed due to the slow dynamics of the pitch control.

In Fig. 21, it can be observed that despite the wind speed variation and the sudden increase in power generation, the DC link voltage is maintained at its reference value due to the rapid response of the current control.

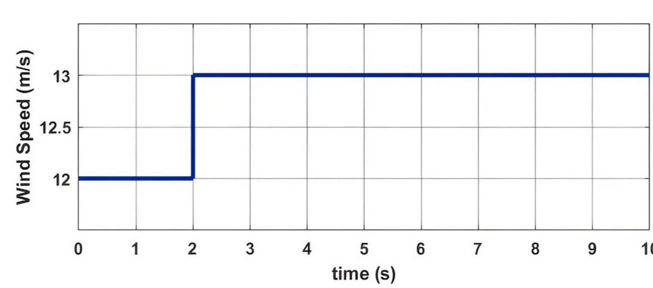

Fig. 16. Step from rated wind speed to wind speed above rated: Wind speed.

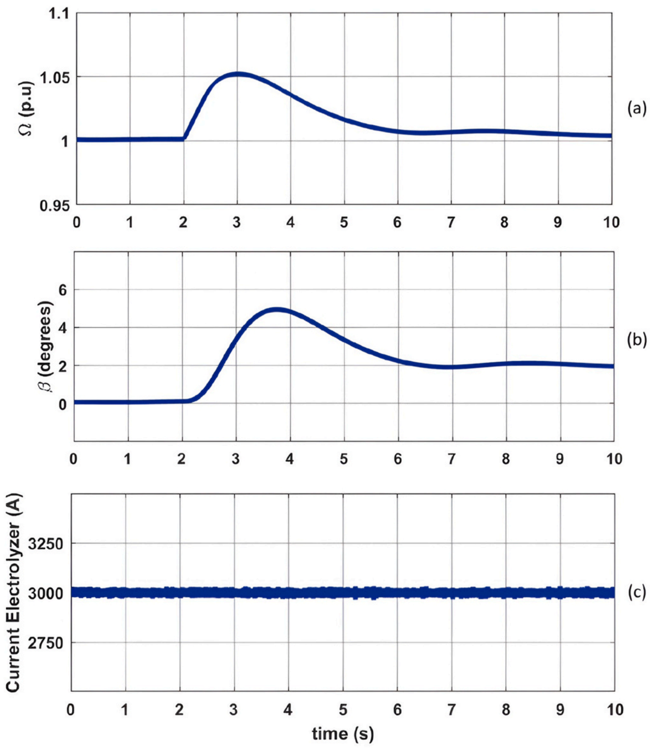

Fig. 17. Step from rated wind speed to wind speed above rated: (a) Rotational Speed (Ω). (b) Blade Pitch Angle (β). (c) Electrolyzer Current.

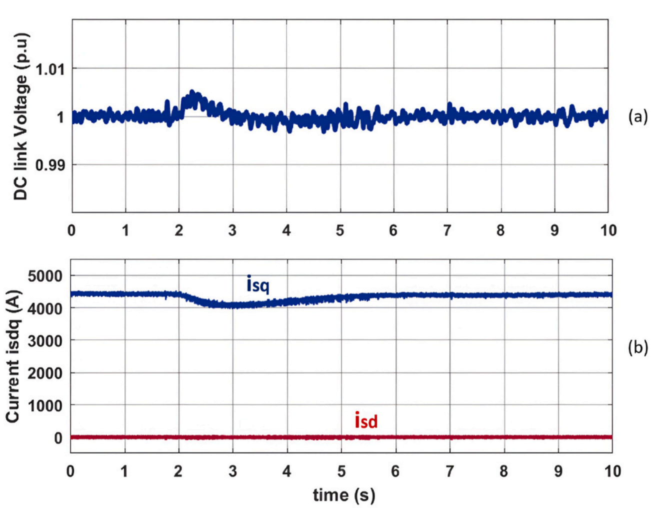

Fig. 18. Step from rated wind speed to wind speed above rated: (a) DC link Voltage. (b) PMSG stator currents in dq.

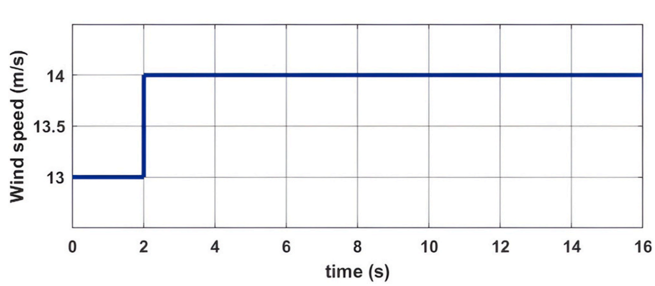

Fig. 19. Step over rated wind speed: Wind speed.

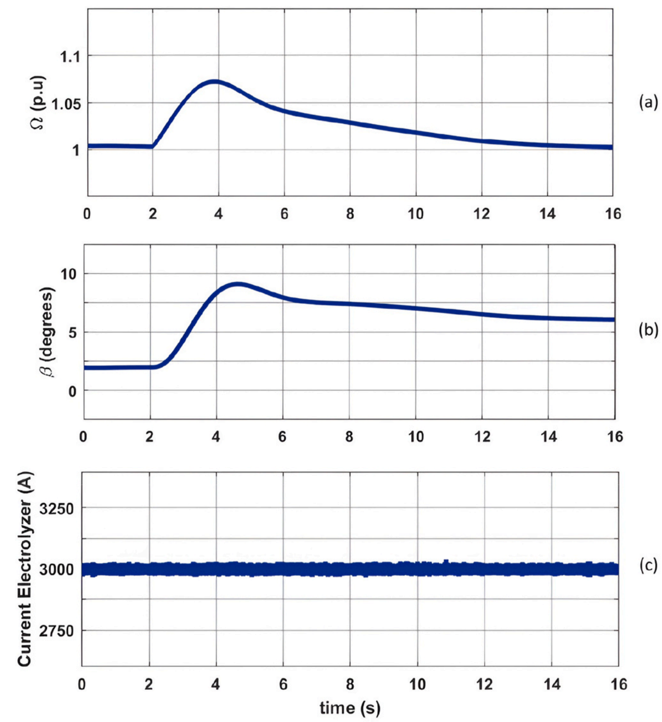

Fig. 20. Step over rated wind speed: (a) Rotational Speed (Ω). (b) Blade Pitch Angle (β). (c) Electrolyzer Current.

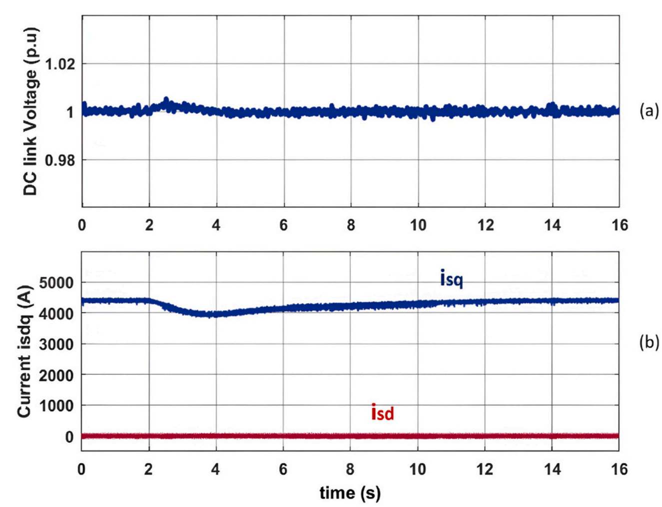

Fig. 21. Step over rated wind speed: (a) DC link Voltage. (b) PMSG stator currents in dq.

As observed in both, this simulation and the previous one, pitch control is slower than the ESC control. This difference in speed arises from the fact that the blade pitch angle actuator is a mechanical actuator limited to $\pm 10^{\circ}/s$ to prevent excessive mechanical loads on the blades. The ESC control and the electrolyzer current remain saturated for the entire simulation, as the rotational speed equals or exceeds their maximum values.

4.5. Step from partial load to full power

In this simulation scenario, a wind speed step from partial load to full power is being tested. The step goes from below the rated wind speed to above it (see Fig. 22). The WT will initially operate at 27.7 rpm and 1.16 MW. The wind speed changes from 11 m/s to 13 m/s at t = 2 s. The

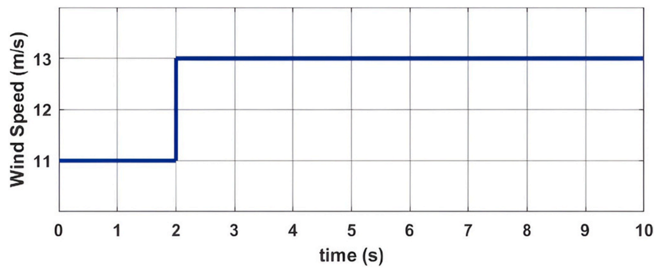

Fig. 22. Step from partial load to full power: Wind speed.

objective of this simulation is to test the coordination between ESC and WT controls.

As shown in Fig. 23, at t = 2 s, the rotational speed begins to rise due to the power increase. When the wind speed changes to 13 m/s, the Ω_{ref} value saturates at its maximum (1 p.u), and due to the ESC control, the electrolyzer current decreases to accelerate the WT and rapidly reach Ω_{ref}. Then, when the rotational speed is close to Ω_{ref}, the electrolyzer current increases until reaching its maximum value. Once the rotational speed crosses 1 p.u, the pitch control is automatically activated. Finally, the blade pitch angle is adjusted until Ω is limited at its maximum value.

In Fig. 24, a small disturbance in the DC-link voltage can be observed. The disturbance occurs at t = 2 s when the wind speed increases, leading to a power imbalance between the WT and the electrolyzer.

As demonstrated in previous simulations, the DC-link voltage disturbance is rapidly dissipated due to the control of the stator current q-component.

4.6. Variable wind speed

In this last simulation scenario, the complete system will be tested using a variable wind speed profile. The WT will initially operate at its nominal rotational speed (30.18 rpm) and nominal power (1.5 MW).

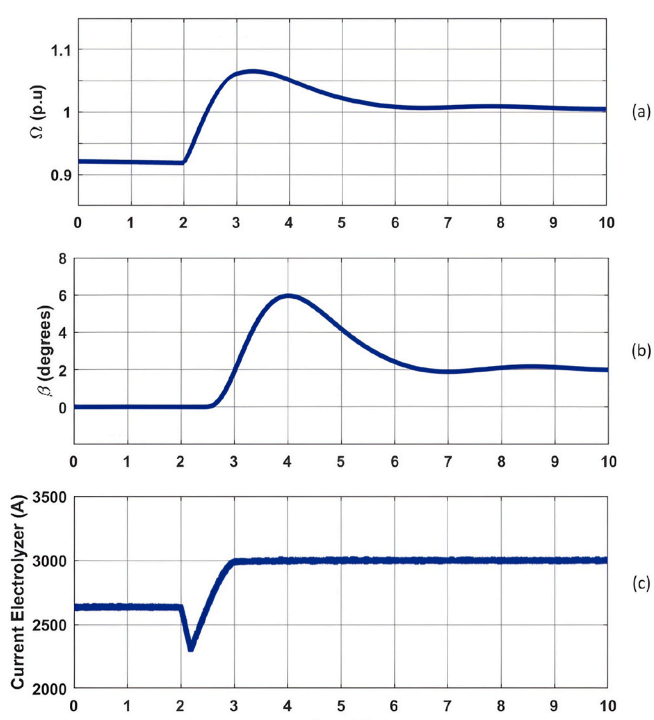

Fig. 23. Step from partial load to full power: (a) Rotational Speed (Ω). (b) Blade Pitch Angle (β). (c) Electrolyzer Current.

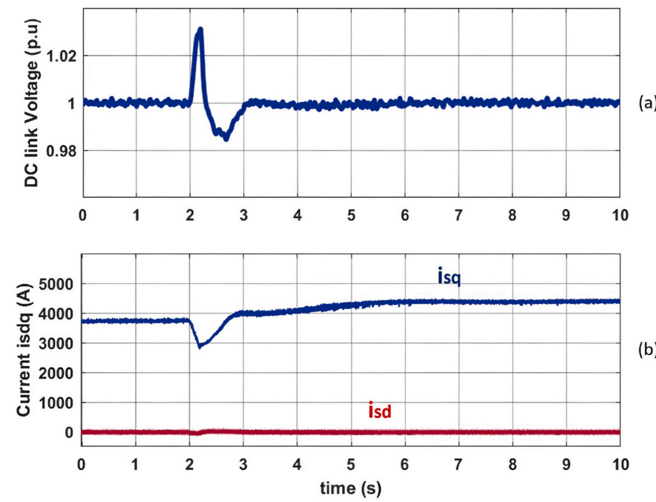

Fig. 24. Step from partial load to full power: (a) DC link Voltage. (b) PMSG stator currents in dq.

The objective of this simulation is to validate the complete system control, including WT, ESC, and GSC controls and observe how the wind turbine, blade pitch angle, AEL, and the different subsystems respond to variable wind speeds. The wind speed will change, as illustrated in Fig. 25, both exceeding the rated value and operating below it.

As shown in Figs. 25 and 26, the wind speed operates below its rated value until t = 35 s. During this period, the rotational speed changes in response to the WT's MPPT by controlling the electrolyzer current consumption, while the blade pitch angle remains at 0°. It is important to note that the electrolyzer current experiences sudden changes due to the constant wind speed fluctuations.

At t = 35 s, the wind speed tends to exceed its rated value, and the pitch control starts limiting the rotational speed at its maximum value. The electrolyzer current is also maintained at its maximum value. Finally, the WT experiences variations in wind speed below and above its nominal value, and the system control continues to operate in the same manner as explained before.

As shown in Fig. 27, the DC link voltage is maintained at its reference value by controlling the q-component of PMSG currents. Recall that maintaining a constant DC link voltage means that the generator supplies exactly the power demanded by the electrolyzer, being this power the wind turbine maximum power for the incident wind velocity when this is below nominal or the wind turbine maximum capacity power when wind velocity is over nominal.

This simulation validates the entire system controls for a variable wind speed situation that is close to the real behavior of an isolated WECS for green hydrogen production.

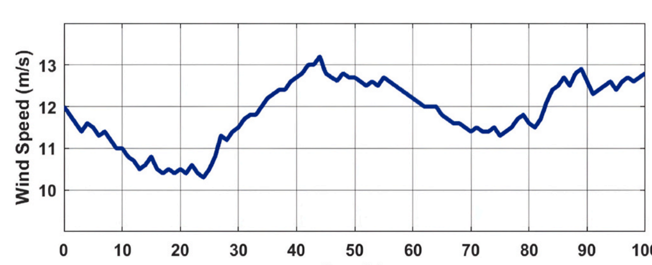

Fig. 25. Variable wind speed: Wind speed.

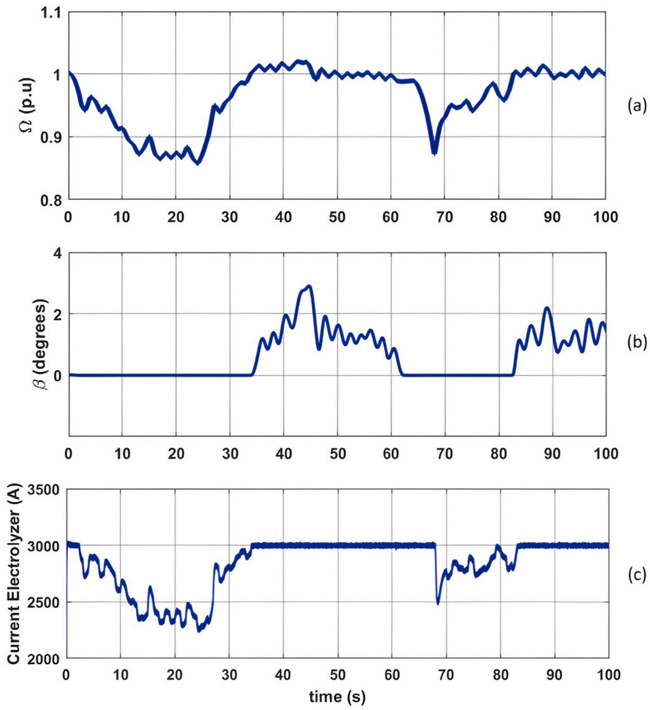

Fig. 26. Variable wind speed: (a) Rotational Speed (Ω). (b) Blade Pitch Angle (β). (c) Electrolyzer Current.

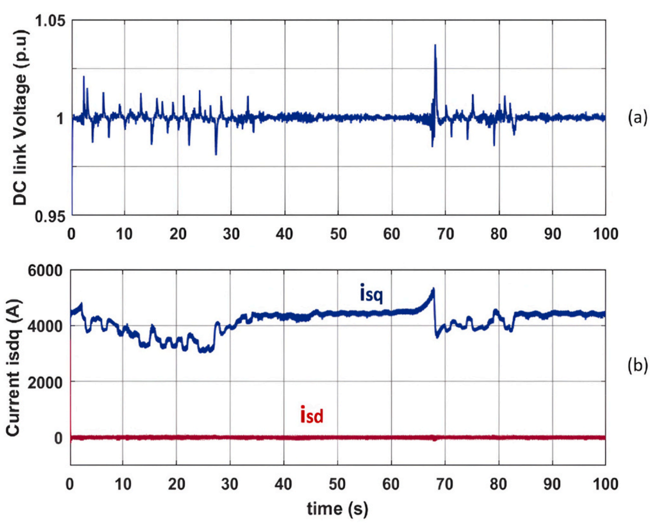

Fig. 27. Variable wind speed: (a) DC link Voltage. (b) PMSG stator currents in dq.

5. Conclusions

This paper introduces a novel WECS system control for isolated green hydrogen production. The system effectively integrates a PMSG wind turbine with an AEL, utilizing a VSC as a Generator Side Converter (GSC) to maintain the DC link voltage at a constant reference value, which on the other hand assures the system power balance. Additionally, it incorporates a Buck Converter as an Electrolyzer Side Converter (ESC) to regulate the current consumption of the electrolyzer, optimizing the WT electrical power production.

Three control systems have been implemented to operate the system. The WT control limits both the rotational speed and mechanical power of the wind turbine to their respective maximum values when wind speed is over rated. The GSC control maintains the DC-link voltage at its reference value under power fluctuations in the system, by controlling the q-component of the PMSG currents providing that the power generated by generator equals the power demanded by the electrolyzer. The ESC control operates as the WT MPPT, controlling the current consumption of the electrolyzer to absorb the power produced by the WT.

Although similar approaches to the one presented in this research have been considered for dimensioning, economic viability, and optimization studies, the control and technical feasibility of these systems have not been properly addressed in the literature. The main contribution of this research lies in the proposed control system, wherein the electrolyzer operates as a controlled load, ensuring the balance of power in the system and enabling the generation of maximum power from the wind energy conversion system without the use of any energy storage systems.

The proposed system and control have been validated on a simulated workbench. Simulation results demonstrate the response of the proposed control system under variable wind speeds, proving its capability to operate properly under power fluctuations. Furthermore, this novel WECS system control also demonstrates its capability to operate the electrolyzer as a controlled load, ensuring power balance in the system and enabling the generation of maximum power from the WECS without energy storage systems, distinguishing it from state-of-the-art proposed systems. This reduces the cost of energy and, consequently, the overall production cost of H2.

However, it is important to note that the electrolyzer experiences abrupt current changes. The adverse effects of these sudden current changes will be studied in future work, and the possible implementation of energy storage systems could provide a solution to stabilize the electrolyzer current under variable wind speeds.

CRediT authorship contribution statement

Eduardo Rausell: Navarro, Writing – review & editing, Writing – original draft, Visualization, Validation, Software, Resources, Project administration, Methodology, Investigation, Formal analysis, Data curation, Conceptualization. **Santiago Arnaltes:** Gómez, Writing – review & editing, Writing – original draft, Supervision, Project administration, Methodology, Investigation, Funding acquisition, Formal analysis, Conceptualization. **José Luis Rodríguez:** Amenedo, Supervision, Resources, Project administration, Investigation, Funding acquisition, Formal analysis, Conceptualization. **Marcos Lafoz:** Pastor, Validation, Supervision, Project administration, Investigation, Funding acquisition, Conceptualization. **Gustavo Navarro:** Soriano, Writing – review & editing, Writing – original draft, Validation, Supervision, Resources, Methodology, Investigation, Funding acquisition, Formal analysis, Data curation, Conceptualization.

Declaration of competing interest

The authors declare that they have no known competing financial interests or personal relationships that could have appeared to influence the work reported in this paper.

Acknowledgments

This paper is part of the R&D project" GREENH2CM para el posicionamiento estratégico de la Comunidad de Madrid en el ámbito de la I + D + i sobre hidrogeno verde y pilas de combustible" funded by Community of Madrid, MCIN/AEI/10.13039/501100011033 and, as appropriate, by "ERDF A way of making Europe", by the "European Union NextGenerationEU/PRTR".

Appendix A. Supplementary data

Supplementary data to this article can be found online at https://doi.org/10.1016/j.ijhydene.2024.06.347.

References

[1] Morante J.R., Andreu T., García G., Guilera J., Tarancón A., Torrel M. Hidrógeno. Vector energético de una economía descarbonizada - Fundación Naturgy 1:47.
[2] Youssef N, Antar y A. Hydrogen generation by water electrolysis. 2018. https://doi.org/10.5772/intechopen.76814.
[3] Hoja de Ruta del Hidrógeno: Una apuesta por el Hidrógeno Renovable.
[4] Commitee and the committe of the regions a hydrogen strategy for a climate-neutral Europe".
[5] Rausell E, et al. "Analysis of using MMC topologies for the direct integration of renewable generation with modular electrolyzers,". In: 2023 25th European conference on power electronics and applications. Aalborg, Denmark: EPE'23 ECCE Europe; 2023. p. 1–8. https://doi.org/10.23919/EPE23ECCEEurope58414.2023.10264620.
[6] Hofrichter Andreas, Rank Daniel, Heberl Michael, Sterner Michael. Determination of the optimal power ratio between electrolysis and renewable energy to investigate the effects on the hydrogen production costs. Int J Hydrogen Energy 2023;48(5):1651–63. https://doi.org/10.1016/j.ijhydene.2022.09.263. ISSN 0360-3199.
[7] Ibáñez-Rioja Alejandro, Järvinen Lauri, Puranen Pietari, Kosonen Antti, Ruuskanen Vesa, Hynynen Katja, Ahola Jero, Kauranen Pertti. Off-grid solar PV–wind power–battery–water electrolyzer plant: simultaneous optimization of component capacities and system control. Appl Energy 2023;345:121277. https://doi.org/10.1016/j.apenergy.2023.121277. ISSN 0306-2619.
[8] Tebibel H. Battery energy storage system for enhancing the electrolyzer capacity factor in small-scale WindtH2 system with a smoothing control strategy: constrained multi-objective Pareto optimization and case study in Algeria. J Energy Storage 2022;52(Part C):105017. https://doi.org/10.1016/j.est.2022.105017. ISSN 2352-152X.
[9] Koponen J, Ruuskanen V, Kosonen A, Niemelä M, Ahola J. "Effect of converter topology on the specific energy consumption of alkaline water electrolyzers,". In: IEEE transactions on power electronics, 34; July 2019. p. 6171–82. https://doi.org/10.1109/TPEL.2018.2876636. 7.
[10] Alhaj Omar Fuad. A new approach for improving the efficiency of the indirectly coupled photovoltaic-electrolyzer system. Int J Hydrogen Energy 2023;48(24):8768–82. https://doi.org/10.1016/j.ijhydene.2022.11.327. ISSN 0360-3199.
[11] Mustafa Ergin S. ahin, A photovoltaic powered electrolysis converter system with maximum power point tracking control. Int J Hydrogen Energy 2020;45(Issue 16):9293–304. https://doi.org/10.1016/j.ijhydene.2020.01.162. ISSN 0360-3199.
[12] García-Valverde R, Miguel C, Martínez-Béjar R, Urbina A. Optimized photovoltaic generator–water electrolyser coupling through a controlled DC–DC converter. Int J Hydrogen Energy 2008;33(20):5352–62. https://doi.org/10.1016/j.ijhydene.2008.06.015. ISSN 0360-3199.
[13] Clarke RE, Giddey S, Ciacchi FT, Badwal SPS, Paul B, Andrews J. Direct coupling of an electrolyser to a solar PV system for generating hydrogen. Int J Hydrogen Energy 2009;34(6):2531–42. https://doi.org/10.1016/j.ijhydene.2009.01.053. ISSN 0360-3199.
[14] Zhou M, Liu Y. "Theoretical study on direct coupling of a PV array to a PEM electrolyser,". In: 2013 international conference on materials for renewable energy and environment, chengdu, China; 2013. p. 52–6. https://doi.org/10.1109/ICMREE.2013.6893613.
[15] Cai Xin, Lin Rui, Xu Ji, Yin Lu. Construction and analysis of photovoltaic directly coupled conditions in PEM electrolyzer. Int J Hydrogen Energy 2022;47(10):6494–507. https://doi.org/10.1016/j.ijhydene.2021.12.017. ISSN 0360-3199.
[16] Bhende CN, Mishra S, Malla SG. " permanent magnet synchronous generator-based standalone wind energy supply system,". IEEE Trans Sustain Energy Oct. 2011;2(4):361–73. https://doi.org/10.1109/TSTE.2011.2159253.
[17] Deng F, Liu D, Chen Z, Su P. "Control strategy of wind turbine based on permanent magnet synchronous generator and energy storage for stand-alone systems,". Chinese Journal of Electrical Engineering 2017;3(1):51–62. https://doi.org/10.23919/CJEE.2017.7961322.
[18] Malla SG, Bhende CN. Voltage control of stand-alone wind and solar energy system. Int J Electr Power Energy Syst 2014;56:361–73. https://doi.org/10.1016/j.ijepes.2013.11.030. ISSN 0142-0615.
[19] Xia J, Chen J, Wang P. "Operation control method of the wind- solar-energy storage dominated islanded microgrid used for hydrogen production,". In: 2023 IEEE 2nd international power electronics and application symposium. Guangzhou, China: PEAS; 2023. p. 651–6. https://doi.org/10.1109/PEAS58692.2023.10395167.
[20] Ishaq Haris, Dincer Ibrahim, Crawford Curran. A review on hydrogen production and utilization: challenges and opportunities. Int J Hydrogen Energy 2022;47(62):26238–64. https://doi.org/10.1016/j.ijhydene.2021.11.149. ISSN 0360-3199.
[21] ENTSO-E publishes a study on flexibility from power-to-hydrogen (P2H2). n.d. https://www.entsoe.eu/2022/06/28/entso-e-publishes-a-study-onflexibility-from-power-to-hydrogen-p2h2/; June 19, 2024.
[22] Zivar D, Kumar S, Foroozesh J. Underground hydrogen storage: a comprehensive review. Int J Hydrogen Energy 2021. https://doi.org/10.1016/J.IJHYDENE.2020.08.138.
[23] Tavakoli SD, Dozein MG, Lacerda VA, Mane MC, Prieto-Araujo E, Mancarella P, Gomis-Bellmunt O. Grid-forming services from hydrogen electrolyzers. IEEE Trans Sustain Energy 2023. https://doi.org/10.1109/TSTE.2023.3270295.
[24] Zheng Y. Power-to-Hydrogen systems: modelling, operation and techno-economic analysis. DTU Wind and Energy Systems 2023. https://doi.org/10.11581/DTU.00000270.
[25] Ulleberg Øystein. Modeling of advanced alkaline electrolyzers: a system simulation approach. Int J Hydrogen Energy 2003;28(1):21–33. https://doi.org/10.1016/S0360-3199(02)00033-2. ISSN 0360-3199.
[26] Bechmann A, Barlas T, Frandsen HL, Jin L, N. Nakashima R. The Hydrogen Wind Turbine: design of a wind turbine optimized for hydrogen production. In: Nejad AR, editor. WindEurope annual event 2023, 2507. IOP Publishing; 2023. https://doi.org/10.1088/1742-6596/2507/1/012010. Article 012010.
[27] Zheng Y, Huang C, Tan J, You S, Zong Y, Træholt C. Off-grid wind/hydrogen systems with multi-electrolyzers: optimized operational strategies. Energy Convers Manag 2023;295. https://doi.org/10.1016/j.enconman.2023.117622. Article 117622.
[28] Chen M, Chou SF, Davari F Blaabjerg y P. Overview of power electronic converter topologies enabling large-scale hydrogen production via water electrolysis. Appl Sci 2022;12(4 feb). https://doi.org/10.3390/APP12041906. de.
[29] Chinchilla M, Arnaltes S, Burgos JC. "Control of permanent magnet generators applied to variable-speed wind-energy systems connected to the grid,". IEEE Trans Energy Convers March 2006;21(1):130–5. https://doi.org/10.1109/TEC.2005.853735.
[30] Heier Siegfried. Grid integration of wind energy conversion systems. John Wiley & Sons Ltd; 1998. ISBN 0-471-97143-X.
[31] Peña Asensio A, Arnaltes Gómez S, Rodriguez-Amenedo JL, García Plaza M, Eloy-García Carrasco J, Alonso-Martínez de las Morenas JM. A voltage and frequency control strategy for stand-alone full converter wind energy conversion systems. Energies 2018;11:474. https://doi.org/10.3390/en11030474.
[32] Qin S, Chang Y, Xie Z, Li S. Improved virtual inertia of PMSG- based wind turbines based on multi-objective model-predictive control. Energies 2021;14:3612. https://doi.org/10.3390/en14123612.
[33] Lamy Claude, Millet Pierre. A critical review on the definitions used to calculate the energy efficiency coefficients of water electrolysis cells working under near ambient temperature conditions. J Power Sources 2020;447:227350. https://doi.org/10.1016/j.jpowsour.2019.227350. ISSN 0378-7753.
[34] Philipp Lettenmeier, Efficiency-electrolysis white paper, siemens gamesa.
[35] Zhou Tao, Bruno Francois. Modeling and control design of hydrogen pro-duction process for an active hydrogen/wind hybrid power system. Int J Hydrogen Energy 2009;34(1):21–30. https://doi.org/10.1016/j.ijhydene.2008.10.030. ISSN 0360-3199.
[36] Peña Asensio A, Gómez SA, Rodriguez-Amenedo JL, Cardiel-Álvarez MÁ. " decentralized frequency control for black start of full-converter wind turbines,". IEEE Trans Energy Convers March 2021;36(1):480–7. https://doi.org/10.1109/TEC.2020.3011611.
[37] Arnaltes S, Rodriguez-Amenedo JL, Montilla-D Jesus ME. Control of variable speed wind turbines with doubly fed asynchronous generators for stand-alone applications. Energies 2018;11:26. https://doi.org/10.3390/en11010026Arnaltes.
[38] Heo SY, Kim MK, Choi JW. Hybrid intelligent control method to improve the frequency support capability of wind energy conversion systems. Energies 2015;8:11430–51. https://doi.org/10.3390/en81011430.
[39] Brice Beltran, Mohamed Benbouzid, Ahmed-Ali Tarek, Mangel Hervé. DFIG-based wind turbine robust control using high-order sliding modes and a high gain observer. International Review on Modelling and Simulations 2011;4(3):1148–55. ⟨hal-00630436v2⟩.